Braz J Phys (2013) 43:247–253
DOI 10.1007/s13538-013-0148-8

SOCIEDADE BRASILEIRA DE FÍSICA

NUCLEAR PHYSICS

Study on $^{222-226}$Th Isotopes in the Cranking Framework

Daya Ram · Rani Devi · S. K. Khosa

Received: 23 August 2012 / Published online: 27 June 2013

Abstract The yrast spectra, quadrupole moments, quadrupole deformation parameters (β_2), non-axiality parameters (γ), root mean-square radii for protons and neutrons, occupation probabilities, moment of inertia (I), and B(E2) transition probabilities are calculated for $^{222-226}$Th in the cranked Hartree–Bogoliubov framework. The calculations employ a quadrupole-quadrupole plus pairing model of residual interaction operating in a reasonably large valence space outside the ^{164}Pb core. Our calculations reproduce qualitatively the observed yrast spectra in $^{222-226}$Th up to spin 20^+. The calculated results indicate that the non-axiality parameter decreases as one moves along the yrast states. The observed increase in deformation from ^{222}Th to ^{226}Th is due to the increase in the occupation of low-k components of $(2g_{9/2})_\pi$ and $(1j_{15/2})_\nu$ orbits. The model parameters reproduce not only the moment of inertia, deformation, and transition probabilities but also the proton and neutron pairing gaps and are the most appropriate for cranking studies in this region.

Keywords Cranked Hartree–Bogoliubov · Yrast spectra · Quadrupole moments

JEL Classification 21.10.Re · 21.60.-n · 27.90.+b

1 Introduction

The known isotopes of thorium range in mass number from 209 to 238. ^{232}Th, the most stable isotope, with a half-life of 14.05 billion years, constitutes nearly all natural thorium. By contrast, ^{209}Th has a half-life of 7 ms. The development of an instability in Th isotopes as A is decreased from 232 to 209 indicates that the nuclear structural properties change with A and depend strongly on the neutron and proton configurations in the underlying valence orbits.

The postulates of quantum mechanics associate the properties of a nuclear system with its wave function, a solution of the Schrodinger-like equation including a two-body residual interaction. Appropriate choices of the two-body interaction should lead to wave functions reproducing the properties of the isotopes under study. In practice, the two-body residual interaction is defined by a model, the parameters of which have to be adequately chosen. Accordingly, we have chosen the schematic quadrupole-quadrupole plus pairing model (PPQ) of the two-body interaction and employed it to obtain the ground-state band properties of $^{222-226}$Th. An important result of our work is the set of interaction parameters, which can now be used to calculate the properties of other Th isotopes and of other mass chains in the neighboring mass region. The optimization of those parameters provided the central motivation for our work.

Azmal et al. [1] and Cocks et al. [2] have studied the spectroscopy of Th isotopes via multinucleon transfer reactions. The positive parity bands in $^{222-226}$Th have been extended up to high spins. Diab [3] investigated the low-lying collective levels in thorium nuclei in the framework of the interacting boson approximation-1 and successfully reproduced the ground state and octupole bands. Egido and Ring [4] have carried out an exact number-projected cranked Hartree–Fock–Bogoliubov calculations with the PPQ interaction for high-spin behavior of the yrast line of well-deformed actinide nuclei. They have discussed several versions of the cranking model, that is, a self-consistent

D. Ram · R. Devi (✉) · S. K. Khosa
Department of Physics and Electronics, University of Jammu, Jammu, 180006, Jammu and Kashmir, India
e-mail: rani_rakwal@yahoo.co.in

calculation without number projection (with and without quadrupole pairing), a full variation after number projection, and a calculation with frozen deformation and gap parameters. They found that the cranking model in the simplified version of the rotating shell model is able to reproduce rather well the alignment and band-crossing pattern along the yrast line in the heavy actinide region.

The cranked Woods–Saxon–Bogoliubov method has been applied to the rotational spectrum of thorium nuclei by Nazarewicz and Olanders [5], who discussed the influence of octupole deformation on high-spin properties of nuclear spectra. Even-even thorium nuclei have also been studied by Zamfir and Kusnezov [6] in the framework of the spdf interacting boson model, and they found that the properties of the low-lying states can be understood without stable octupole deformation. As the low-lying states in light thorium isotopes can be understood without stable octupole deformation, and these nuclei have not been studied with the PPQ interaction, we have employed the non-axial cranking framework to study the properties of $^{222-226}$Th by the PPQ interaction model. The PPQ model has been extensively used by Kumar and Baranger to study the nuclear deformation in the rare-earth region [7–11]. This model was applied for the first time in conjunction with cranked HFB framework by Ring et al. [12] to certain rare-earth nuclei.

Self-consistent cranking calculations in the framework of nonrelativistic density functional theories have been performed by various groups [13–15]. Fleckner et al. [13] have self-consistently calculated the rotational states in the rare-earth region with the Skyrme interaction, and their calculations in the lower-spin region ($J \leq 20$) showed qualitative agreement with PPQ calculations and experiment. Bonche et al. [14] have obtained a three-dimensional solution of cranked Hartree–Fock plus BCS equations. On the basis of several parameterizations of the Skyrme interactions, they showed that the complete yrast line of ^{24}Mg supports the notion that rotational properties are primarily determined by properties of the interaction connected with multipole deformations for $\ell \geq 2$. Egido and Robledo [15] used the Gogny force for the first time to carry out self-consistent cranked mean-field Hartree–Fock–Bogoliubov (HFB) calculations and applied it to the well-known nucleus ^{164}Er. Koepf and Ring [16] applied covariant density functional theory by using the concept of the cranking model to describe rotational nuclei. They investigated the yrast line of ^{20}Ne.

Here, we present a non-axial study on $^{222-226}$Th isotopes in the cranked Hartree–Bogoliubov (CHB) framework. Within this framework, we calculate the yrast states, intrinsic quadrupole moments, deformation parameters (β_2), non-axiality parameters (γ), root mean-square radii for protons (r_π) and neutrons (r_ν), occupation probabilities, moment of inertia (I), and B(E2) transition probabilities. In the variational calculation of the yrast levels, we have employed the usual PPQ effective interaction operating in a valence space spanned by the $3p_{1/2}$, $3p_{3/2}$, $2f_{5/2}$, $2f_{7/2}$, $2g_{9/2}$, $1h_{9/2}$, $1i_{11/2}$, $1i_{13/2}$, and $1j_{15/2}$ orbits for protons as well as for neutrons. The nucleus ^{164}Pb has been chosen as an inert core.

Our choice of the interaction parameters and core is seen to reproduce the spherical nature of ^{208}Pb and the shell closure for $Z = 82$ and $N = 126$, indicating therefore that the parameter set and valence space are suitable for cranking calculations in the mass region $A \sim 220$. The results indicate that the increased collectivity as one moves from ^{222}Th to ^{226}Th is due to an increase in the occupation of the $(2g_{9/2})_\pi$ and $(1j_{15/2})_\nu$ orbits. The observed deformation increases from ^{222}Th to ^{224}Th because the occupation of the $(1j_{15/2})_\nu$ orbit rises from 4 to 6. And the increased deformation from ^{224}Th to ^{226}Th is linked with the rising occupation of the $(2g_{9/2})_\pi$ orbit from 0.06 to 0.11.

The paper is organized as follows. In Section 2, an outline of the CHB formalism is given, and the results obtained from the present calculations are discussed in Section 3. Finally, the various conclusions drawn from the present analysis are presented in Section 4.

2 Calculational Details

The CHB formalism has been discussed in detail by Goodman [17]. Consider the many-body Hamiltonian

$$H = \sum_i \langle i|T|i\rangle a_i^\dagger a_i + \frac{1}{4}\sum_{ijkl}\langle i,\, j|V_A|k,l\rangle a_i^\dagger a_j^\dagger a_l a_k, \qquad (1)$$

where T is the kinetic energy and V_A is an effective nucleon–nucleon interaction. The indices i, j, k, l span the active valence single-particle states in the model space, and $a_i^\dagger$ and a_i denote particle creation and annihilation operators, respectively. The cranking model for number of nonconserving wave functions replaces H by

$$H' = H - \lambda N - \omega J_x, \qquad (2)$$

where the angular frequency is adjusted so that

$$\langle J_x\rangle = \sqrt{J(J+1)}, \qquad (3)$$

and the chemical potential λ is adjusted to yield the correct expectation value of the number operator N.

We have employed the single-particle energies (in mega-electron volts) $(2f_{7/2})$=0, $(1h_{9/2})$=0.5, $(1i_{13/2})$=1.9, $(3p_{3/2})$=2.4, $(2f_{5/2})$=2.9, $(3p_{1/2})$=3.9, $(2g_{9/2})$=5.8, $(1i_{11/2})$ =7.5, and (1j15/2)=7.8, taken from the Nilsson diagram http://ie.lbl.gov/toipdf/nilsson.pdf.

The two-body effective interaction in our computation is of the PPQ type [7–11]. The pairing part can be written in the form

$$V_P = \frac{G}{4} \sum_{i,j} S_i S_j a_i^\dagger a_{\bar{i}}^\dagger a_{\bar{j}} a_j \tag{4}$$

where i denotes the quantum numbers $(nljm)$. The state $\bar{i}$ is same as i, except that the sign of m is reversed. S_i denotes the phase factor $(-1)^{j-m}$. The $q-q$ part of the interaction is given by the equality

$$V_{qq} = \frac{\chi}{2} \sum_{ijkl} \sum_{\nu} \langle i|q_\nu^2|k\rangle \langle j|q_{-\nu}^2|l\rangle (-1)^\nu a_i^\dagger a_{\bar{j}}^\dagger a_l a_k, \tag{5}$$

where the operator q_ν^2 is given by the expression

$$q_\nu^2 = \sqrt{\frac{16\pi}{5}} r^2 Y_\nu^2(\theta, \phi). \tag{6}$$

The chosen strengths of the like-particle neutron-neutron (χ_{nn}) or proton–proton(χ_{pp}) interactions, in units of MeVa^{-4}, are $-0.0056, -0.0055$, and -0.0052 for $^{222-226}$Th, respectively. The chosen strength of the neutron–proton χ_{np} interaction is 1.7 times $\chi_{nn} = \chi_{pp}$. The effective interaction χ_{np} tends to deform the nucleus, while $\chi_{nn} = \chi_{pp}$ tends to pair [18–23]. These ideas have played a pivotal role in the development of the stretch scheme of Danos and Gillet [21], rotor model of Arima and Gillet [22], and interacting boson model of Arima et al. [23]. These considerations have led us to the choice $\chi_{np} = 1.7\chi_{nn}$, i.e., larger than χ_{nn}. We have fixed the strength of the pairing interaction by the empirical relation (18-21)/A [24]. This set of interaction parameters not only reproduces the difference $E_{2^+} - E_{0^+}$ but also the experimental $B(E2; 0_1^+ \rightarrow 2_1^+)$ for $^{222-226}$Th. In addition, the pairing gap parameters for protons and neutrons for $^{222-226}$Th are comparable to those in Ref. [25] for the same nuclei. The set of interaction parameters is parametrized by the relations

$$\chi_{nn} = \chi_{pp} = -(10-11) \times A^{-1.4}\,\mathrm{MeV}a^{-4}, \tag{7}$$

and

$$\chi_{np} = 1.7 \times \chi_{nn}. \tag{8}$$

with

$$G = (18-21)/A. \tag{9}$$

Here, $a = \sqrt{\hbar/m\omega}$ is the oscillator parameter. The like-particle effective interaction in Eq. 7 and G in Eq. 9 yield optimized parameters reproducing the moment of inertia, the deformation, the B(E2) transition probabilities, and the pairing gap parameters in these nuclei. Tables 1 and 2 show good agreement between the computed and experimental values for these physical quantities. In our calculations, the core is ^{164}Pb, which was chosen because our code uses the same valence space for protons and neutrons. To verify that the parameters are reliable and the core, adequate, we have carried out a CHB calculation for ^{208}Pb. The calculated components of the quadrupole moments for protons and neutrons are zero, reproducing the shell closure for neutron number 126. This successful test encouraged us to use the same parameter set for all subsequent investigations in this region.

Table 1 Comparison between the experimental (Exp.) and calculated (Theor.) energy gap $E_{2^+} - E_{0^+}$ and pairing gaps for protons (Δ_π) and neutrons (Δ_ν), in mega-electron volts. The experimental data are from Refs. [2, 25, 26, 30]

	^{222}Th	^{224}Th	^{226}Th
$E_{2^+} - E_{0^+}$ (Exp.)	0.183	0.098	0.072
$E_{2^+} - E_{0^+}$ (Theor.)	0.184	0.115	0.101
Δ_π(Exp.)	1.08	0.94	0.87
Δ_π(Theor.)	1.34	1.24	1.04
Δ_ν(Exp.)	0.93	0.74	0.57
Δ_ν(Theor.)	1.07	0.76	0.50

3 Results and Discussion

Our results determine the yrast states, intrinsic quadrupole moments, β_2, γ, root mean-square radii for protons and neutrons, occupation probabilities, moment of inertia (I), and B(E2) transition probabilities of $^{222-226}$Th isotopes in the non-axial CHB framework. In spite of its several shortcomings, this formalism has been extensively used to study the complexity of nuclear spectra, due to the interplay of single-particle and collective aspects of nuclear motion, as a function of rotational frequency. Here, we study transitional light $^{222-226}$Th nuclei.

3.1 Results of the Calculation for $^{222-226}$Th Isotopes

3.1.1 ^{222}*Th*

Figure 1 compares the yrast spectra of ^{222}Th, calculated up to spin $J = 20^+$, with experimental data [26]. The experimental yrast energies are well reproduced. The experimental value of E_{20^+} is 3.60 MeV, and the theoretical value is 4.05 MeV. The calculated intrinsic quadrupole moments are presented in Table 3, the two components $\langle Q_0^2\rangle$ and $\langle Q_2^2\rangle$ of the quadrupole moments being separately presented for protons and neutrons. It turned out in our calculation that $\langle Q_2^{-2}\rangle = \langle Q_2^2\rangle$ and $\langle Q_1^2\rangle = \langle Q_{-1}^2\rangle = 0$. The tabulated values grow along the yrast states. We have calculated β_2 from the intrinsic quadrupole moments with the expression

Table 2 Comparison between theoretical and experimental $B(E2; 0_1^+ \rightarrow 2_1^+)$ and β_2 for $^{222-226}$Th. The effective proton charge is $e_\pi = 1 + e_{\text{eff}}$, and the effective neutron charge is $e_\nu = e_{\text{eff}}$. The experimental data are from Refs. [26, 28, 30, 31]

	Nucleus	Exp.	Theor.		
			$e_{\text{eff}} = 0.50$	$e_{\text{eff}} = 0.65$	$e_{\text{eff}} = 0.80$
β_2	^{222}Th	0.153(8)	0.156	0.183	0.210
	^{224}Th	0.21	0.163	0.190	0.218
	^{226}Th	0.228(7)	0.168	0.196	0.225
$B(E2; 0_1^+ \rightarrow 2_1^+)(e^2b^2)$	^{222}Th	2.95(28)	3.17	4.33	5.66
	^{224}Th	3.88(28)	3.48	4.75	6.22
	^{226}Th	6.85(42)	3.75	5.12	6.70

suggested by Raman et al. [27]. We have obtained $\beta_2 = 0.156$ for ^{222}Th, with the value 0.153 adopted by Raman et al. [28] for effective charge $e_{\text{eff}} = 0.5$. Columns 4 and 6 in Table 3 show that, for ^{222}Th, $\langle Q_2^2 \rangle$ slowly decreases along the yrast states. The parameter γ measures the non-axiality of a nucleus. This parameter is obtained from $\langle Q_2^2 \rangle$ by means of an expression suggested by Bohr [29]. The calculated values slightly decrease with spin. The last two columns of Table 3 show the root mean-square radii for protons and neutrons. The r_π is smaller than the r_ν as one proceeds along the yrast states. The r_ν is nearly constant along the yrast states, whereas r_π slightly increases as one moves along the yrast states. Thus, the results for $\langle Q_0^2 \rangle$ and γ show increasing quadrupole collectivity and decreasing non-axiality along the yrast states of this nucleus.

3.1.2 ^{224}Th

Experimental data for the yrast band of ^{224}Th are available up to $J = 18^+$; our calculations run up to 20^+. The experimental data come from Ref. [30]. The calculated yrast spectra in Fig. 1 reproduce the experimental yrast energies with reasonable accuracy. For example, the experimental energy for the 2^+ state is 0.098 MeV, whereas the calculated energy is 0.115 MeV. For the highest spin, that is, 18^+, the experimental energy is 2.864 MeV, whereas the calculated value is 3.125 MeV. The intrinsic quadrupole moments for this nucleus are presented in Table 3. The moments $\langle Q_0^2 \rangle_{\pi,\nu}$ grow along the yrast states. The calculated value of β_2 for this nucleus is 0.218 when $e_{\text{eff}} = 0.80$ is used, whereas the Raman et al. [31] have adopted the value 0.21. The growing $\langle Q_0^2 \rangle_{\pi,\nu}$ shows that the quadrupole collectivity rises along

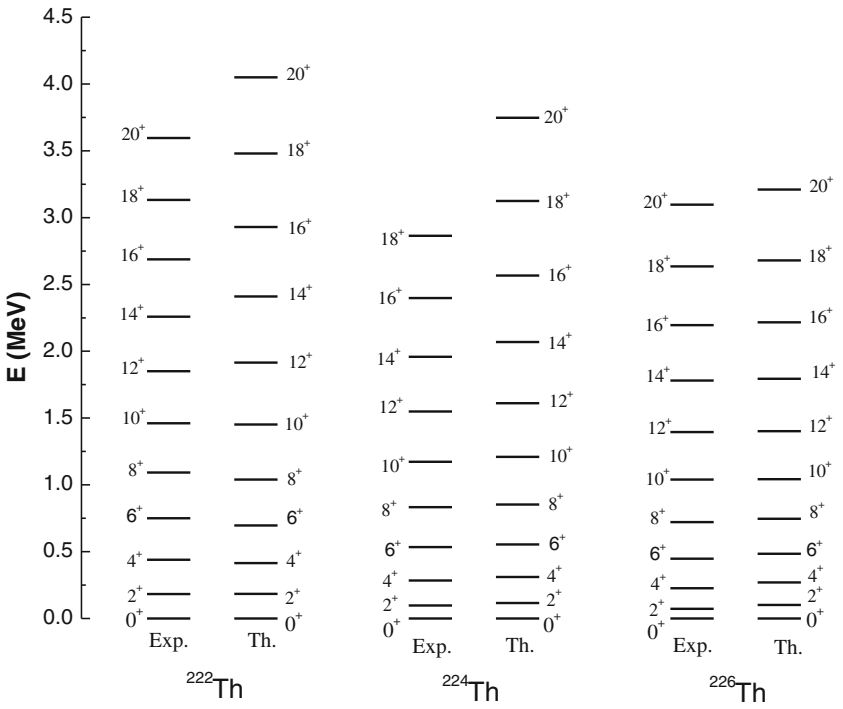

Fig. 1 Comparison between experimental and calculated yrast spectra for $^{222-226}$Th. The experimental data are taken from references [2, 26, 30]

Table 3 Results of CHB calculations for the $^{222-226}$Th isotopes. Here, $\langle Q_0^2\rangle_\pi$, ($\langle Q_0^2\rangle_\nu$), and $\langle Q_2^2\rangle_\pi$ ($\langle Q_2^2\rangle_\pi$) give the contribution of the protons (neutrons) to the components of quadrupole moment operator. The quadrupole moments have been calculated in units of b (barn). The 7th column lists γ, the degree of non-axiality. The r_π (r_ν) in columns 8th and 9th are the root mean-square radii for protons (neutrons) in fermis

Nucleus	J	$\langle Q_0^2\rangle_\pi$	$\langle Q_2^2\rangle_\pi$	$\langle Q_0^2\rangle_\nu$	$\langle Q_2^2\rangle_\nu$	γ	r_π	r_ν
	0	2.472	0.987	3.840	4.359	−56.90	6.46	6.62
	2	2.473	0.987	3.840	4.357	−56.88	6.48	6.62
	4	2.475	0.985	3.840	4.353	−56.83	6.50	6.62
	6	2.478	0.982	3.841	4.346	−56.75	6.52	6.62
	8	2.482	0.978	3.841	4.337	−56.65	6.53	6.62
^{222}Th	10	2.487	0.974	3.841	4.326	−56.52	6.55	6.62
	12	2.492	0.968	3.842	4.312	−56.37	6.56	6.62
	14	2.498	0.962	3.842	4.296	−56.19	6.57	6.62
	16	2.504	0.955	3.843	4.278	−55.99	5.58	6.62
	18	2.511	0.947	3.844	4.256	−55.77	6.59	6.62
	20	2.515	0.942	3.845	4.231	−55.50	6.59	6.62
	0	2.585	0.973	4.044	4.462	−56.24	6.47	6.66
	2	2.586	0.972	4.045	4.521	−56.22	6.49	6.66
	4	2.588	0.971	4.046	4.456	−56.17	6.50	6.66
	6	2.590	0.968	4.047	4.449	−56.10	6.52	6.66
	8	2.594	0.965	4.049	4.439	−55.99	6.53	6.66
^{224}Th	10	2.599	0.961	4.051	4.427	−55.87	6.54	6.66
	12	2.604	0.957	4.054	4.412	−55.72	6.56	6.66
	14	2.611	0.950	4.058	4.394	−55.53	6.57	6.66
	16	2.617	0.945	4.061	4.375	−55.34	6.58	6.66
	18	2.625	0.938	4.066	4.352	−55.12	6.58	6.66
	20	2.633	0.931	4.071	4.326	−54.86	6.59	6.66
	0	2.688	0.930	4.182	3.844	−52.90	6.48	6.66
	2	2.689	0.930	4.182	4.026	−52.88	6.50	6.65
	4	2.690	0.929	4.183	3.837	−52.84	6.51	6.65
	6	2.691	0.927	4.185	3.830	−52.77	6.52	6.65
	8	2.694	0.924	4.188	3.820	−52.67	6.54	6.65
^{226}Th	10	2.697	0.921	4.191	3.807	−52.54	6.55	6.65
	12	2.700	0.917	4.195	3.791	−52.39	6.56	6.65
	14	2.704	0.912	4.200	3.773	−52.21	6.57	6.65
	16	2.709	0.907	4.206	3.752	−52.01	6.58	6.65
	18	2.713	0.901	4.211	3.729	−51.77	6.59	6.65
	20	2.720	0.894	4.220	3.699	−51.50	6.60	6.65

the yrast states. The γ calculated from the components of quadrupole moments decreases along the yrast states. The root mean-square radii in the last two columns show that the r_π increases along the yrast states and is smaller than the r_ν.

3.1.3 ^{226}Th

The experimental level scheme of ^{226}Th has been obtained by Cocks et al. [2]. The positive-parity yrast band is known up to spin 20^+. The yrast spectra of ^{226}Th has been obtained up to spin 20^+ and is compared with the experimental data in Fig. 1. The experimental yrast energies are well reproduced by the CHB calculations. For example, for the 20^+ state, the experimental energy is 3.097 MeV, whereas the calculated value is 3.210 MeV. The deviation is only 0.113 MeV. The intrinsic quadrupole moment components $\langle Q_0^2\rangle$ in the third and fifth columns of Table 3 grow with spin along the yrast states. The calculated β_2 for this nucleus is 0.225 when $e_{\text{eff}} = 0.80$ is used, whereas the value adopted by Raman et al. [28] is 0.228(7). The non-axiality parameters (γ) calculated from the $\langle Q_2^2\rangle$ components of the intrinsic quadrupole moments also decrease with spin. Therefore, also in ^{226}Th, the quadrupole collectivity increases, whereas the non-axiality diminishes along the yrast states. The root mean-square radii in the last two columns of Table 3 increase with spin, whereas the r_ν is

Table 4 Calculated occupation numbers for various proton and neutron orbits in the ground state of $^{222-226}$Th

Nucleus	$3p_{1/2}$	$3p_{3/2}$	$2f_{5/2}$	$2f_{7/2}$	$2g_{9/2}$	$1h_{9/2}$	$1i_{11/2}$	$1i_{13/2}$	$1j_{15/2}$
Protons									
^{222}Th	0.32	0.81	0.61	2.17	0.06	2.09	0.0004	1.94	0
^{224}Th	0.34	0.81	0.63	2.15	0.07	2.07	0.0005	1.92	0
^{226}Th	0.34	0.81	0.66	2.15	0.11	2.03	0.0006	1.89	0
Neutrons									
^{222}Th	1.46	2.60	3.85	7.08	5.46	9.01	4.52	12.02	4.00
^{224}Th	1.46	2.60	3.84	7.08	5.46	9.01	4.52	12.02	6.00
^{226}Th	1.43	2.98	4.58	7.50	5.33	9.51	4.41	12.26	6.00

nearly constant along the yrast states. The r_π is smaller than the r_ν.

3.2 Subshell Occupation Number

Table 4 presents the subshell occupation numbers for protons and neutrons. The occupation numbers of various proton orbits are spread over $3p_{1/2}$, $3p_{3/2}$, $2f_{5/2}$, $2f_{7/2}$, $2g_{9/2}$, $1h_{9/2}$, and $1i_{13/2}$ orbits. The occupation probabilities of the $3p_{1/2}$, $2f_{5/2}$, and $2g_{9/2}$ orbits grow, whereas the occupation probabilities of $2f_{7/2}$, $1h_{9/2}$, and $1i_{13/2}$ orbits slowly decay from ^{222}Th to ^{226}Th. The growing occupation of the $(2g_{9/2})_\pi$ orbit, from 0.06 to 0.11, makes the deformation grow from ^{224}Th to ^{226}Th.

Consider next the occupation numbers for neutrons. The occupation probability of the $1j_{15/2}$ orbit grows from 4 to 6 units between ^{222}Th and ^{224}Th, incrementing the quadrupole deformation. The growth of the quadrupole deformation is also observed experimentally, as the energy $E_{2_1^+}$ decreases to 0.098 MeV in ^{224}Th, from 0.18 MeV in ^{222}Th.

3.3 B(E2) Transition Probabilities

To check the quality of the CHB wave function, we calculated $B(E2; 0_1^+ \to 2_1^+)$. The intrinsic quadrupole moments have been shown [27, 28, 32, 33] to be related to the $B(E2; 0_1^+ \to 2_1^+)$ by the equality

$$B\left(E2; 0_1^+ \to 2_1^+\right) = \frac{5}{16\pi}\begin{bmatrix}0 & 2 & 2\\ 0 & 0 & 0\end{bmatrix}^2 \left[e_\pi \langle Q_0^2\rangle_\pi + e_\nu \langle Q_0^2\rangle_\nu\right]^2 e^2 b^2. \tag{10}$$

Table 2 compares the observed $B(E2; 0_1^+ \to 2_1^+)$ with the values resultant from the substitution of the quadrupole moment components of $^{222-226}$Th in Table 3 for $\langle Q_0^2\rangle_\pi$ and $\langle Q_0^2\rangle_\nu$ on the right-hand side of Eq. 10. The effective proton charge e_π is $1 + e_{\text{eff}}$, and the effective neutron charge e_ν is e_{eff}. The calculated $B(E2; 0_1^+ \to 2_1^+)$ for $^{222-226}$Th agrees

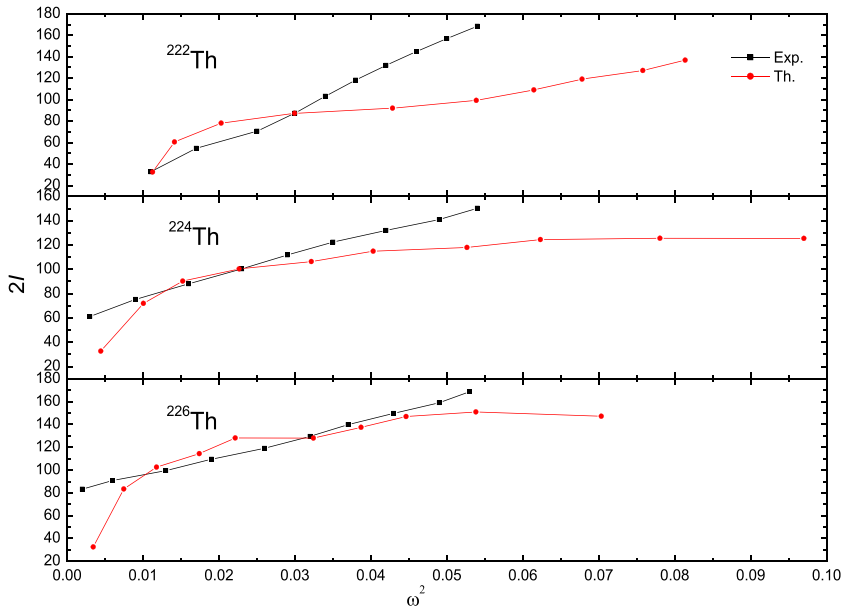

Fig. 2 Moment of inertia I versus the square of the cranking frequency ω^2 for the yrast spectra of $^{222-226}$Th

well with the experimental data for the effective charges ranging from 0.50 to 0.80 in our study. For example, the experimental $B(E2; 0_1^+ \rightarrow 2_1^+)$ for ^{222}Th is $2.95(28)e^2b^2$, while the theoretical value is $3.17e^2b^2$ for $e_{\text{eff}} = 0.50$.

3.4 Moment of Inertia

Figure 2 shows the experimental and theoretical plots of the moments of inertia I and square of the cranking frequency ω^2 for the $^{222-226}$Th nuclei. I and ω^2 have been computed from the yrast energies, to which they are related by the following expressions: [34]:

$$\frac{2I}{\hbar^2} = \frac{4J-2}{E_J - E_{J-2}} \quad \left[(\text{MeV})^{-1}\right], \tag{11}$$

and

$$(\hbar\omega)^2 = \frac{(J^2 - J + 1)(E_J - E_{J-2})}{(2J-1)^2} \quad \left[(\text{MeV})^{-1}\right]. \tag{12}$$

Figure 2 shows that the experimental variation of I as a function of ω^2 increases with spin. The theoretical results for the variation of I as a function of ω^2 also increase with spin and qualitatively follow the experimental trend.

4 Conclusions

To summarize, our CHB calculations on the basis of the quadrupole-quadrupole plus pairing model of the residual interaction operating in reasonably large valence space well describes the positive-parity yrast bands of even-even $^{222-226}$Th isotopes. The calculations confirm the non-axial nature of these isotopes. The quadrupole deformation grows, and the non-axiality of all these nuclei decreases along the yrast states. The root mean-square radii for protons and neutrons show that neutrons have greater probability than protons to constitute the surface of $^{222-226}$Th. The computed occupation numbers link the growth in collectivity from ^{222}Th to ^{226}Th with increasing occupation of the $(2g_{9/2})_\pi$ and $(1j_{15/2})_\nu$ orbits. The observed deformation growth from ^{222}Th to ^{224}Th is due to increased occupation of the $(1j_{15/2})_\nu$ orbit, from 4 to 6. Further, the increased deformation from ^{224}Th to ^{226}Th is linked with the increased occupation of the $(2g_{9/2})_\pi$ orbit, from 0.06 to 0.11. The experimental B(E2) transition probabilities for $^{222-226}$Th are reproduced when effective charges in the range 0.50 to 0.80 are used. Last, but not the least, our calculation reports an optimized set of interaction parameters for the PPQ interaction model of interaction, expected to well describe the nuclear structure in this mass region.

Acknowledgments We gratefully acknowledge the team of reviewers of the *Brazilian Journal of Physics* for their valuable suggestions that have enhanced the quality of the present paper. One of the authors (DR) is grateful to UGC, New Delhi, India, for providing a financial assistance under RGNJRF no. F. 14-2(SC)/2010(SA-III).

References

1. N. Azmal et al., J. Phys. G. Nucl. Part. Phys. **25**, 831 (1999)
2. J.F.C. Cocks et al., Nucl. Phys. **A645**, 61 (1999)
3. S.M. Diab, Prog. Phys. **2**, 97 (2008)
4. J.L. Egido, P. Ring, Nucl. Phys. **A423**, 93 (1984)
5. W. Nazarewicz, P. Olanders, Nucl. Phys. **A441**, 420 (1985)
6. N.V. Zamfir, D. Kusnezov, Phys. Rev. **C63**, 054306 (2001)
7. M. Baranger, K. Kumar, Nucl. Phys. **62**, 113 (1965)
8. M. Baranger, K. Kumar, Nucl. Phys. **A110**, 490 (1968)
9. K. Kumar, M. Baranger, Nucl. Phys. **A110**, 529 (1968)
10. K. Kumar, M. Baranger, Nucl. Phys. **A122**, 241 (1968)
11. K. Kumar, M. Baranger, Nucl. Phys. **A122**, 273 (1968)
12. P. Ring, R. Beck, H.J. Mang, Z. Phys. **231**, 10 (1970)
13. J. Fleckner, U. Mosel, P. Ring, H.J. Mang, Nucl. Phys. **A331**, 288 (1979)
14. P. Bonche, H. Flocard, P.H. Heenen, Nucl. Phys. **A467**, 115 (1987)
15. J.L. Egido, L.M. Robeldo, Phys. Rev. Letts. **70**, 2876 (1993)
16. W. Koepf, P. Ring, Nucl. Phys. **A493**, 61 (1989)
17. A.L. Goodman, Nucl. Phys. **A230**, 466 (1974)
18. P. Federman, S. Pittel, Phys. Lett. **B69**, 385 (1977)
19. S.C.K. Nair, A. Ansari, Satpathy, Phys. Lett. **B71**, 257 (1977)
20. S. Pittel, Nucl. Phys. **A347**, 417 (1980)
21. M. Danos, V. Gillet, Phys. Rev. **161**, 1034 (1967)
22. A. Arima, V. Gillet, Ann. Phys. (N.Y.) **66**, 117 (1971)
23. A. Arima, T. Otsuka, F. Iachello, I. Talmi, Phys. Lett. **B66**, 205 (1977)
24. D.R. Bes, R.A. Sorensen, in *Advances in Nuclear Physics*, vol. 2, ed. by M. Baranger, E. Vogt (Plenum, New York, 1969), p. 129
25. S. Pilat, K. Pomorski, A. Staszczak, Z. Phys. **A332**, 259 (1989)
26. S. Singh, A.K. Jain, J.K. Tuli, Nucl. Data Sheets **112**, 2851 (2011)
27. S. Raman, C.W. Nestor Jr., K.H. Bhat, Phys. Rev. **C37**, 805 (1988)
28. S. Raman, C.W. Nestor Jr., P. Tikkanen, At. Data Nucl. Data Tables **78**, 1 (2001)
29. A. Bohr, Mat. Fys. Medd. K.Dan Vidensk. Selsk. **26**, 14 (1952)
30. A.A. Cohen, Nucl. Data Sheets **80**, 227 (1997)
31. S. Raman, C.H. Malarkey, W.T. Milner, C.W. Nestor Jr., P.H. Stelton, At. Data Nucl. Data Tables **36**, 1 (1987)
32. G. Ripka, in *Advances in Nuclear Physics*, vol. 1, ed. by M. Baranger, E. Vogt (Plenum, New York, 1968)
33. C.G. Adler, M.K. Banerjee, G.J. Stephenson, Bull. Am. Phys. Soc. **13**, 581 (1968)
34. P.N. Tripathi, S.K. Sharma, S.K. Khosa, Phys. Rev. **C29**, 1951 (1984)